24th COBEM - 2017

24th ABCM International Congress of Mechanical Engineering
December 3-8, 2017, Curitiba, PR, Brazil

COBEM-2017-1647
ROBOTIC PLATFORM WITH PASSIVE SUSPENSION TO BE APPLIED ON SOYBEAN CROPS: INITIAL RESULTS

Vitor Akihiro Hisano Higuti
Andres Eduardo Baquero Velasquez
University of São Paulo, Av Trabalhador São-Carlense, 400, São Carlos, São Paulo, Brazil
vitor.higuti@usp.br, andresbaquero@sc.usp.br

Mateus Valverde Gasparino
Gustavo Capalbo de Oliveira
Caio Ian Alher Carrasco
José Carlos Risardi
Daniel Varela Magalhães
Marcelo Becker
University of São Paulo, Av Trabalhador São-Carlense, 400, São Carlos, São Paulo, Brazil
mateus.gasparino@usp.br, gustavo.capalbo.oliveira@usp.br, caio.carrasco@usp.br, jcrisard@sc.usp.br, daniel@sc.usp.br, becker@sc.usp.br

Débora Marcondes Bastos Pereira Milori
Embrapa Instrumentation, Rua XV de Novembro, 1452, São Carlos, São Paulo, Brazil.
debora.milori@embrapa.br

Abstract. *The main objective of this work is to present the development and characteristics of a robotic platform to be applied on a soybean crop, which has the goal of inspecting and detecting diseases in soybean crops, either in an autonomous or semi-autonomous way. This paper describes the design process of the robotic platform, showing final images of the robot drawings; its main characteristics, including calculations used to define such characteristics; and the embedded devices, which consists of the necessary electronics to control the motors, the sensors used to navigate in the crop, and the processing unit. Also, some initial tests are presented to determine if a Light Detection and Ranging (LiDAR) sensor and a Microsoft Kinect could be used to detect a soybean plant in any growth stage of the plant. For the design of the robotic platform, the growth process and the main characteristics (row spacing, space between plants of the same crop row and plant height) of the soybean crops, in Brazil, are exhibited.*
Keywords*: Precision Agriculture, Mobile Robot, Mechanical Design*

1. INTRODUCTION

According to the United Nations forecasts, the global population is growing from the current 7.3 billion people to approximately 9.7 billion until 2050, even with a deceleration of fertility (United Nations, 2015). This data, together with the situation that approximately 795 million people are globally undernourished (FAO, 2015), confirms the projections of Food and Agriculture Organization of the United Nations (FAO): the need for a 70% increase in global food production until 2050 (FAO, 2011).

In the same way, a great demand in the production of grains is expected in Brazil for the next years. According to the study (Ministério da Agricultura, Pecuária e Abastecimento, 2016), the grain harvested in Brazil will rise from 196.5 million to 255.3 million tons in the period between the years of 2015 and 2026, an increase of 58.8 million tons (30%), with only soybean being responsible for an increase of 95.6 million to 129.2 million tons (35.1%).

While the expected increase for the production is about 30%, the forecast of expansion for the cultivated area is 12.7%. In other words, the crop yield should be higher even if the cultivated area does not advance at the same rate. This affirmation means that it is necessary an increase of efficiency based on the application of technologies related to the agriculture and also an improvement in the production of labor and capital, which will demand investments in infrastructure, research and financing (Ministério da Agricultura, Pecuária e Abastecimento, 2016).

According to (Freitas, 2011), soybean is one of the most important crops in the world economy, being used in the agro, chemical and food industry. In Brazil, the soybean crops represented 57% (33.17 million of hectares) of the

cultivated area of cereal, vegetables and oilseeds crops in 2015/2016 and 50% (95.63 million of ton) of the total production of cereal, vegetables and oilseed in 2015/2016 (CONAB, 2016).

Although soybean represents an important cultivation for Brazil, there are not known works about robotic platforms used to monitor and detect diseases in soybean crops around world.

For this reason, the Mobile Robotics Laboratory (LabRoM) from São Carlos School of Engineering (EESC) of USP, in partnership with Brazilian Agricultural Research Corporation (EMBRAPA), are developing a ground robotic platform and novel techniques for monitoring field conditions and detecting diseases in soybean crops.

Although Unmanned Aerial Vehicles (UAVs) market has been rapidly increasing in the agriculture, these technologies do not compete as they should provide different types of information. For instance, UAVs significantly improved crop monitoring compared to satellite imagery, previously most advance form of monitoring (Mazur, 2016). Due its operating requirements and also to avoid undesired disturbances to the field, UAVs shall keep a minimum distance from canopy at any stage. Allied to crop growth, these factors undermine the collection of under canopy information such as disease, weed and plagues early detection, soil analysis and plant width. Despite a significant decrease in speed may be expected, a ground robot would be able to carry a larger number of sensors and execute multiple measurements at once compared to the restricted UAV payload, usually few kilograms for commercially available units (Dronelli, 2017).

This paper describes the design process of this robotic platform, its main characteristics, embedded devices and an initial test to determine if a Light Detection and Ranging (LiDAR) sensor and a Microsoft Kinect can be used to detect a soybean plant in any growth stage of the plant.

2. DESCRIPTION OF THE ROBOTIC PLATFORM

The robotic platform is a 4WDS (Four Wheels Drive and Steering) vehicle with passive suspension. Developed by LabRoM and EMBRAPA, its dimensions are based on the main characteristics (row spacing, space between plants of the same crop row and plant's height) of the soybean crops in Brazil. Tab. 1 shows the standard values for each characteristic (Ritchie, 1998; Farias, *et al.*, 2007; EMBRAPA Soja, 2010).

Table 1. Main characteristics of soybean crops in Brazil

Characteristic	Standard Values
Row Spacing	0.4m, 0.45m or 0.5m
Space between plants of the same crop row	0.05 - 0.1m
Plant's height	0 - 1.2m

Three situations were analyzed to choose the robot width. The first one consists in the robot navigating in the middle of two crop rows. This alternative has the problem that the robot's width might be less than 0.5m (maximal standard value for row spacing) and the robot would not have enough space for all required devices. The second alternative is when the robot navigates using three consecutive crop rows: left side wheels between first and second crop rows, while robot's right side wheels navigate between the second and third rows. Thus, the robot body navigates above the second row. This alternative is not possible to use because the robot needs a region free of plants in order to use the Laser-Induced Breakdown Spectroscopy (LIBS) system. This system is embedded inside the robot to monitor the ground characteristics of the crop and it is being developed by researchers of EMBRAPA and USP (Larenas, *et al.*, 2016a; Larenas, *et al.*, 2016b; Larenas, *et al.*, 2016c). The last alternative is that the robot navigates in four consecutive crop rows: left side wheels between the first and second rows, while robot's right side wheels uses the street between third and fourth rows. Thus, the robot body navigates above the space between the second and third row. This allows having enough space inside the robot for the embedded devices, and more importantly, having a region free of plants in order to use the LIBS system. As conclusion of the analysis, the robot will navigate in four consecutive crop rows and therefore, its width will be twice the chosen value for row spacing.

Table 2. Situations analyzed to determine the robot's width

Robot's width (m)	Row Spacing of soybean crop (m)	Maximal space for wheel navigation (m)
1	0.45	0.17
	04	0.1
0.9	0.5	0.2
	0.4	0.15
0.8	0.5	0.15
	0.45	0.17

As there are three possible values for row spacing (see Tab.1) and the robot width is twice the value for row spacing of the soybean crop, then it is necessary to choose one of them and use it to set robot width. For this, three situations were analyzed. Each situation considers that the robot is designed with a width equal to twice the value of some row spacing shown in Table 1 and the robot navigates in soybean crops with row spacing equal to the other two values. For each situation, it was analyzed the maximal, internal or external, space that the robot's wheels have to navigate. All analyses are presented in Tab. 2.

The value for robot's width that has more space for wheel navigation for soybean crops with any value of row spacing, is 0.9m. For this reason, this value is the selected width for the robot. To select the robot's height, it is necessary to define if the robot can navigate in soybean crops in any growth stage. According to Heiffig, *et al.* (2006), the percentage of closure between lines, for soybean crops with different row spacing, changes according to the growth stage of the crop. Table 3 presents the percentage value for soybean crops, with different row spacing, in different growth stages.

Table 3. Percentage of closure between lines of soybean crops (Heiffig, *et al.*, 2006)

Growth Stage / Row Spacing	V7	R1	R2	R3	R5	R6
0.4m	65.3%	82.1%	89%	96.9%	99.2%	100%
0.5m	55.9%	76.4%	87.9%	93.6%	96.1%	99.7%

According to Mundstock and Thomas (2005), the growth process for soybean plants is divided in vegetative and reproductive growth stages. The vegetative stages are labeled with V and the reproductive stages with R (Farias, *et al.*, 2007). The vegetative stages describe the development of the soybean plant from seeding to flowering period. The two initial vegetative stages are Emergence Vegetative stage (VE) and Cotyledons Vegetative stage (VC). VE stage represents the cotyledons emergence and VC represents the stage in which the cotyledons are fully open and expanded (Farias, *et al.*, 2007). From VE stage, the vegetative stages are sequentially numbered like V1, V2, V3, …, Vn where n indicates the number of nodes, above the cotyledon node, with fully developed leaves (Farias, *et al.*, 2007). The reproductive stages describe the development of soybean plant from flowering to maturation period. They cover four different phases of plant reproductive development: flowering (R1 and R2), pod development (R3 and R4), grain development (R5 and R6) and plant maturation (R7 and R8).

According to Table 3, the robot can navigate in soybean crops in growth stages from VC to R1. For these growth stages, the plants' height varies between 0m and 0.46m (Ritchie, 1998; Farias, *et al.*, 2007). Then, the robot height might be greater than 0.46m, leading to a selected height of 0.6m (from the ground to the lowest part of body robot). The robot's length is accordingly selected to generate a square robotic platform, and hence, the length for the robotic platform is 0.9m.

Summarizing, the robotic platform (Fig. 1a and 1b) is a 4WDS vehicle used to monitor and detecting diseases in soybean crops (growth stages from VC to R1) and its dimensions are 0.9m x 0.9m x 0.9m (width, length and height). The structure of the robotic platform is composed by five parts (Fig. (1a)): 1- Steering modules; 2- Suspension system 3- Support for LiDAR sensor and 4- Robot's body.

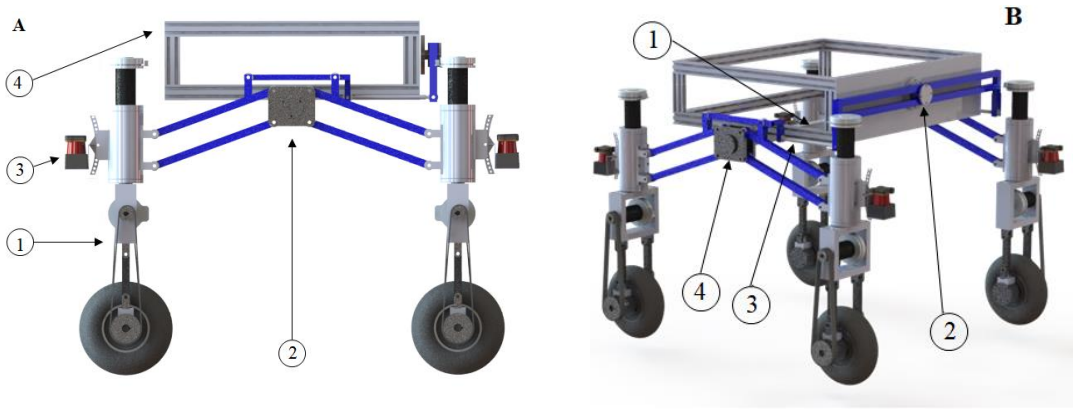

Figure 1. a- Robot parts; b- Suspension system parts.

The robotic platform has four steering modules where the propulsion and steering motors are located, and they are better described in Section 2.1. The robot's body is a rectangular box made with aluminum profile and its dimensions are 0.7m x 0.9m x 0.3m (width, length and height). All required devices (Section 2.2) for the robot are in the robot's body. The robot has four LiDAR supports, and each support is located on the surface of each steering module, 0.4m from ground. These LiDAR supports allow changing the angle between LiDAR reading plane and ground. The last robot part

is the suspension system that is composed by four parts (Fig. 1b): 1- Body axis; 2- Arm to link the two four-bar mechanisms 3- hexagon bars and 4- four-bar mechanism.

The suspension system allows the robot to adapt to the unevenness of the terrain. For this, the robot has two four-bar mechanisms. Each mechanism is composed by two-wheel modules and two sets of steel square tubes (blue bars in Fig. 1b). When an unevenness of the terrain causes some of the wheels to move up or down, then the four-bar mechanism suitably moves in order to keep the wheel modules perpendicular to ground. This movement is transmitted to the other four-bar mechanism, by an arm, in order to keep the other wheel modules perpendicular to ground. All those movements allow the robot body to have the least possible inclination; the other wheels do not lose the contact with the ground and the robot can continue with its forward navigation. The movement of the four-bar mechanism is transmitted to the arm by a hexagon steel bar. The embedded sensors will be described in Section 2.2 and the electrical part will be described in Section 2.3.

2.1 Propulsion and steering sets

For the propulsion and steering sets, the robotic platform has eight brushless EC 90 Flat motors (Maxon part number: 429271) manufactured by Maxon Motor. Four of them are used for the propulsion set and the others for the steering set. The motor's input voltage is 36V, its nominal current is 4.75A and its nominal torque is 560mNm. Each motor has coupled a planetary gearhead GP 52C (Maxon part Number: 223086) and an encoder MILE sensor (Maxon part number: 453234). The gearhead reduction rate is 21:1 and it can support torques between 4-30Nm. The encoder resolution is 512 counts per turn.

The robotic platform has four wheel modules (Fig. 2), each one with two Maxon motors (one for steering and another one for propulsion). Each wheel module is divided in ten parts: 1- Steering motor; 2- Gearhead; 3- Steering system; 4- Protective box for propulsion motor; 5- Pulley coupled to propulsion motor; 6- Fork; 7- Synchronizing belt; 8- Pulley coupled to wheel; 9- Wheel flange housing and 10-Tire with air chamber.

The steering system is composed by a steering shaft (made with 1045 steel), two angular contact ball bearings, one rubber seal, one base for the LiDAR sensor, a mechanism to connect the wheel module to the four-bar mechanism (see blue square tubes in Fig. 1) and an aluminum jacket to protect all parts of the steering system. The gearhead shaft is coupled to the steering shaft in order to transmit the steering motor's movement and torque. In each side of the steering shaft there is an angular contact ball bearing and they are fixed inside the aluminum jacket. In the outer jacket surface, the LiDAR base and the mechanism to connect to the four bars mechanism are fixed. The angular contact ball bearings are manufactured by SKF and their model is 7206. All other pieces of the steering system are designed and manufactured in the University of São Paulo. Considering that the nominal motor torque is 560mNm, the gearhead reduction rate and efficient is 21:1 and 86% respectively, then the torque in the gearhead axis is obtained by the Eq. (1).

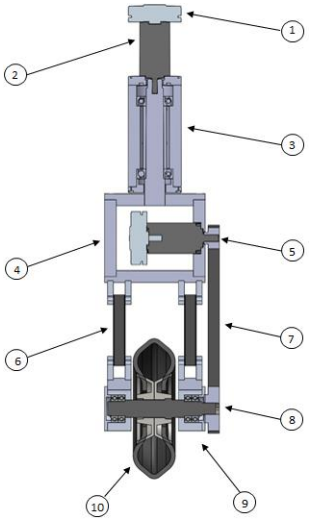

Figure 2. Wheel modules

$$\tau_{Gearhead\_shaft} = \tau_{motor} \times 21 \times 0.86 = 9.67\,Nm \quad (1)$$

As the top side of protective box is fixed in the steering shaft, its bottom side is fixed in the fork and the wheel flange housings are fixed in the fork, then the gearhead torque and movement are transmitted directly from the steering shaft to the wheel flange housings and therefore to the wheel. Each wheel flange housing contains two 6005-zz ball bearings

manufactured by SKF. Such ball bearings supports the wheel shaft that subsequently supports the wheel. The rotation of the propulsion motor is transmitted to the wheel shaft by two pulleys and a synchronizing belt. The first pulley has 10 teeth and it is coupled to the gearhead of the propulsion motor, while the second pulley has 22 teeth and it is coupled to the wheel shaft. As the two pulleys have different teeth number and the wheel pulley has the greater teeth number then there is a transmission relation of 1:2. In other words, the torque on the wheel shaft is twice the torque of propulsion motor (19.52Nm) but the speed of propulsion motor in the gearhead shaft (nominal of 119.52 rpm) is halved and therefore the nominal speed of wheel shaft is 59.76 rpm. Eq. (2) is used to calculate the nominal wheel speed.

$$V_{wheel}\left(\frac{m}{s}\right)=\frac{V_{gearhead\_propulsion}(rpm)}{60s}\times\pi\times r_{wheel}(m)=\left(\frac{59.76rpm}{60s}\right)\times\pi\times 0.125m=0.77\frac{m}{s} \quad (2)$$

Where r_{wheel} is the wheel radius (0.125m). According to Eq. (2), the nominal speed of each robot wheel is 0.77m/s. To calculate the force generated by the propulsion motor on the wheel, Eq. (3) is used

$$F_{wheel}(N)=\frac{2\times\tau_{gearhead\_shaft}}{r_{wheel}}=\frac{2\times 9.76Nm}{0.125m}=156.16N \quad (3)$$

According to Eq. (3), the highest force generated by each wheel is 156.16N. As the robotic platform has four wheels, then its higher propulsion force is 624.64N. Assuming that the robot weight is 120kg (critical value for the robot weight) and the propulsion force is equal to 624.4N (higher propulsion force), the robotic platform can navigate in a terrain with inclination lower than 32.08° (see Eq. (4)).

$$Inclination\_angle(^\circ)=\sin^{-1}\left(\frac{4\times F_{wheel}}{m\times g}\right)=\sin^{-1}\left(\frac{624.64N}{120kg\times 9.8\frac{m}{s}}\right)=32.08^\circ \quad (4)$$

Where m is the robot mass and g is the gravity. According to Höfig and Araujo-Junior (2015), "the soil slope classes were classified according to the potential for mechanization in extremely able (0 to 5%), very able (5.1 to 10%), able (10.1 to 15%), moderately able (15.1 to 20%) and not recommended (> 20%)". Then the proposed robotic platform is capable of navigating in crops with recommended slopes and also in those with not recommended slopes (> 20%).

To control the speed and position of this robotic platform Maxon motors, four ESCON 50/5 boards and four EPOS2 24/5 boards are being used. Propulsion only requires control of the speed of the motor. For such purpose, 4-quadrant PWM servo controller ESCON 50/5 operating in closed loop speed control is chosen to drive the propulsion motors. Its operation voltage range is 10-50V and its highest output current is 15A (Maxon motor, 2015). Conversely, steering requires a finer control of both motor's position and speed to properly provide wheel steering angles. Thus, motion controller EPOS2 24/5 operating in position mode drives the steering motor. Its operation voltage range is 11V-24V and its highest output current is 10A (Maxon motor, 2016).

2.2 Embedded devices

The robotic platform has embedded four LiDAR (Light Detection and Ranging) sensors and a Kinect sensor (manufactured by Microsoft) for scanning the environment. The LiDAR model is UTM-30LX (Teixidó, *et al.*, 2012; Demski, *et al.*, 2013) and it is manufactured by Hokuyo company. As the main unit control, the robotic platform has an ARK 3510 industrial fanless box PC manufactured by Advantech Company and the access to the ARK 3510 is made by a wireless router. For localization, the robot has a GPS (Global Positioning System) receiver whose commercial model is PIKSI (manufactured by Swift Navigation). Finally, the robot has an IMU (Inertial Measurement Unity) whose commercial model is MPU9150 (manufactured by Spark Fun). All embedded devices are described in the following subsections. The communication between the ARK3510 computer and each sensor is via USB. Fig. 4 presents all the embedded devices and sensors of this robotic platform.

2.2.1 Hokuyo UTM – 30LX

The UTM-30LX is a two-dimensional radial scanning laser range finder with an effective sensing range up to 30 meters in indoor and outdoor environments (Pallejá, *et al.*, 2009). Its dimensions are 0.06x0.06x0.087m (width, length and height) and its weight is 0.210kg. Its angular resolution is 0.25° and it has an angular reading range equal to 270°. The light source of the UTM-30LX is a semiconductor laser diode (λ=905nm) and it has a rotating mirror which sweeps

the laser beam horizontally. The mirror rotates at about 2400rpm generating a scan speed of 25ms. The guaranteed distance range for UTM-30LX is 0.1-30m and its power consumption is less than 8W (power supply equal to 12V and current supply equal to 0.7A). The communication between the UTM-30LX and the computer is made by USB interface and its speed is 12Mbps (Hokuyo Automatic Co, 2012).

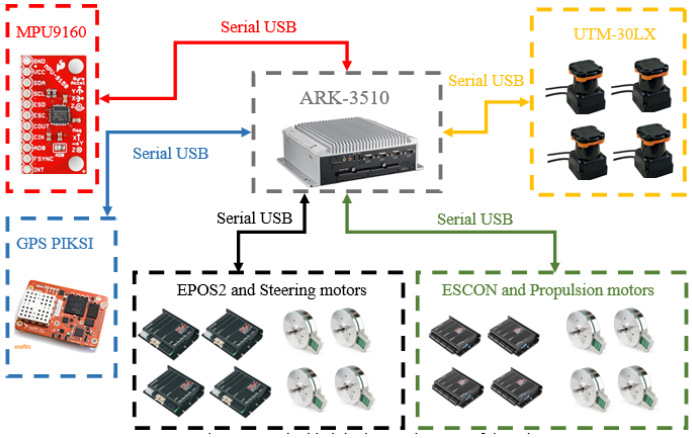

Figure 3. Embedded devices and sensor of the robot

2.2.2 ARK 3510

The ARK-3510 is a fanless box computer with x86 architecture manufactured by Advantech. It has an Intel Core I7-3610Q 2.3GHz quadcore processor, 4GB of RAM memory (DDR3) and a hard disk of 1TB. Its dimensions are 0.29m x 0.09m x 0.232m (width, height and length) and its weight is 4.63kg. To connect external devices, the ARK-3510 has four USB 3.0 ports, two USB 2.0 ports and 4 RS232 serial ports. The power consumption of this computer is less than 60W and its power input voltage is 12V. It is using Linux Ubuntu 14.04 LTS as the operating system, but it can also work using Windows operating system (Advantech, 2016).

2.2.3 Kinect Sensor

According to Han, *et al.*, (2013), "KINECT is an RGB-D sensor providing synchronized color and depth images, and it was initially used as an input device by Microsoft for the Xbox game console". Actually, it is used in some researches about artificial vision due to its low cost. Zhang (2012) said "The Kinect sensor incorporates several advanced sensing hardware. Most notably, it contains a depth sensor, a color camera, and a four-microphone array that provides full-body 3D motion capture, facial recognition, and voice recognition capabilities". Nowadays the Kinect sensor is composed by a RGB (Red Green Blue) camera with a 1280 x 960 resolution, an infrared emitter, an IR depth sensor, four microphones and 3-axis accelerometers. Its frame rate is 30 frames per second and it has vertical and horizontal viewing angles equal to 43° and 57° respectively.

2.2.4 MPU-9150

The MPU-9150 is the world's first 9-axis Motion Tracking MEMS manufactured by Sparkfun. This device was designed for the low power, low cost, and high-performance requirements (Sparkfun, 2015). According to Higuti, *et al.* (2016), "the MPU-9150 combines two chips: the MPU-6050, which contains a 3-axis gyroscope, 3-axis accelerometer, and an onboard Digital Motion Processor™; and the AK8975, a 3-axis digital compass. It is possible to retrieve not only standalone data but also integrated information like RPY (Roll Pitch Yaw) values using an open source firmware". Finally, its communication can be made through I2C bus.

2.2.5 PIKSI GPS receiver

Piksi Multi is a multi-band, multi-constellation RTK (Real Time Kinematic) GNSS (Global Navigation Satellite System) receiver that provides centimeter-level accuracy at a low cost (Swift Navigation, 2017). This GPS receiver is manufactured by Swift Navigation. Its horizontal position and velocity accuracies are 2.5m and 0.03m/s RMS respectively. Its horizontal RTK accuracy is 0.010m+1ppm and its vertical RTK accuracy is 0.015+1ppm. Its dimensions are 0.048m x 0.071m x 0.012m (width, length and height) and its weight is 0.020Kg. This sensor can work in environments with temperatures from -40°C to 85°C. The Piksi has two UART-LVTTL ports, two CAN bus, 1 Gigabit Ethernet port and two USB 2.0 ports (1 Device and 1 Host). Finally, its power consumption is 2.9W and its input voltage range is 5-15V.

2.3 Electric System

This section describes the power consumption of all embedded sensors and devices in order to know the electrical autonomy of the robot. For this, the power consumption of each sensor and device is calculated with Eq. (5) and presented in Table 4.

$$P(W) = V \times I \tag{5}$$

Table 4. Power consumption of each robot embedded device and sensor.

Sensor or Device	Voltage (V)	Nominal Current (A)	Power Consumption (W)
UTM-30LX	12	1	12
ARK 3510	12	5	60
PISKI GPS	5V	0.5	2.5
MPU-9150	5	0.1	0.5
Propulsion Motor + ESCON 50/5	36	4.86	171.55
Steering Motor + EPOS2 24/5	24	4.88	114.65

The batteries used by the robot are lithium batteries of 36V and 10Ah (one battery for each two motors and ESCON or EPOS2 boards). Also, the robot has another battery of 36V and 6.75Ah to supply the other devices and sensors. The power supply of the first batteries is 360Wh and the power supply of the last battery is 243Wh.

Two batteries powers the propulsion subsystem, having each one with 343.1W power consumption (two motors and two ESCON boards). Then the electrical autonomy for the batteries is 63 minutes approximately. Another two batteries are used for the steering subsystem, and each one needs to provide 229.3W (two motors and two EPOS2 24/5 boards). Hence the electrical autonomy for these two batteries is 82 minutes approximately. Moreover, the power consumption of the other devices (LiDAR, IMU, PC and GPS) is 111W. This leads to a 92 minutes electrical autonomy. The robot electrical autonomy is 63 minutes because it is the lowest value for all batteries autonomy.

As there are some devices and sensors whose input voltage is less than 36V, then some voltage regulators are being used. The first case is for the steering motors with their respective EPOS2 board. The power consumption for two motors and two EPOS2 board is 229.3W then it is necessary to use a voltage regulator which can reduce 36V to 24V and supports 230W. In this case, the RSD-300C-24 is being used. Manufactured by Mean Well, its input voltage range is 33.6V to 62.4V and the output power is up to 300W.

The last case is for ARK 3510 and four UTM-30LX LiDAR. The power consumption for these devices is 111W, then it is necessary to reduce the battery voltage from 36V to 12V, supporting at least 111W. For this case, a RSD-150C-12 is being used. This voltage regulator is manufactured by Mean Well, and its input voltage range is from 33.6V to 62.4V and its output power is up to 150W.

Summarizing, the electrical system of the robotic platform is composed by four lithium batteries of 36V and 10Ah, one lithium battery of 36V and 6.75Ah, two voltage regulators whose commercial reference are RSD-300C- 24 and RSD-150C- 12. Finally, the robot electrical autonomy will be 63 minutes.

3. LIDAR AND KINECT TEST

This section describes a test using the LiDAR, a webcam and a Kinect sensors at an experimental soybean crop built in LabRoM's building. This test's goal was to verify the response of these sensors when they are used with soybean plants. The experimental soybean crop (Fig. 4a) consists of a 2m x 0.7m rectangular area, where five soybean rows are planted to contain a sample of each main characteristic (see Tab. 1). The first row (located in the left side of Fig. 5a) had 10 plants per linear meter, the second one had 8 plants per linear meter, the third one had 7 plants per linear meter, the fourth one had 6 plants per linear meter and the last one had 5 plants per linear meter. The row spacing between first and second crop row was 0.4m, the row spacing between second and third crop row was 0.45m, the row spacing between third and fourth crop row was 0.5 and finally the row spacing between the fourth and five crop row was 0.45m. A wood stand was used to support the sensors, replicating their expected places on the robot frame (Fig. 4b). It was build and used exclusively for this test. LiDAR Hokuyo UTM30-LX (1) is placed upside-down 0.4m from ground. Its reading plane has an angle of around 20 degrees with the ground plane; Kinect 360 model 1414 (2): placed on top of the wood stand and Webcam RGB Philips SPC230NC (3): placed below Kinect.

The soybean plants were sowed on November 1st (year 2016) and they were assessed for 50 days. At least every two days in this period, the data collection happened twice a day: one between 8 and 9am (UTC -3) and another between 12 and 1pm (UTC -3). The wood stand is placed on up to five pre-defined spots (Fig. 4a) and relevant measurements are taken:

• In all spots, ten consecutive pictures were taken with Kinect and Webcam using OpenCV for Python 2.7;

• In each one of the spots 2 to 5, a thousand consecutive LiDAR readings (distance and intensity) were taken using URG Network library for C++.

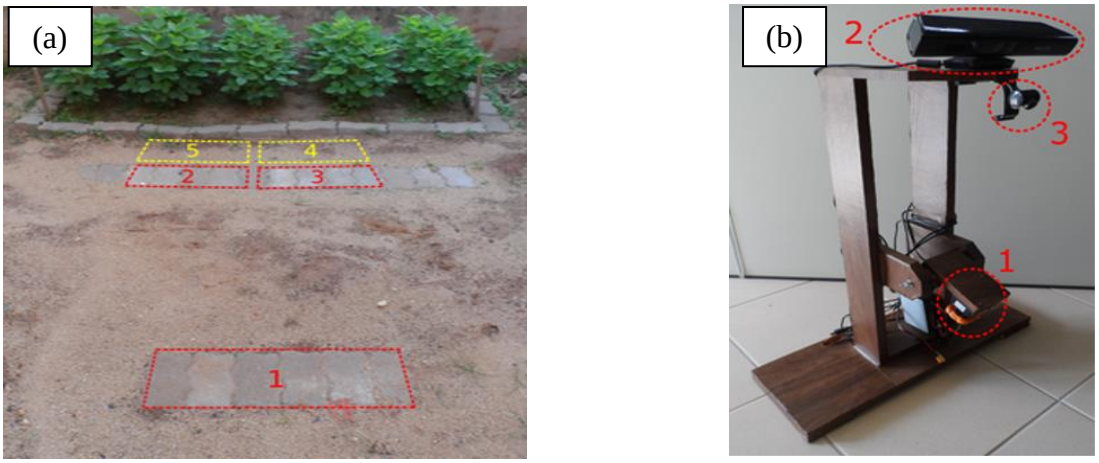

Figure 4. (a) Experimental site with 5 spots where wood stand should be placed; (b) Wood stand.

Figure 5a shows a photo taken with Kinect when the wood stand was located at spot 1 in the second day at 1 pm. As there were no plants emerging from the ground in the second day, then Fig. 5b presents how the LiDAR detects the ground when there are not plants. The red graphic in Fig. 5b shows the LiDAR intensity of the ground. This graphic is the reference to determine if the LiDAR detects or not a plant in the other days.

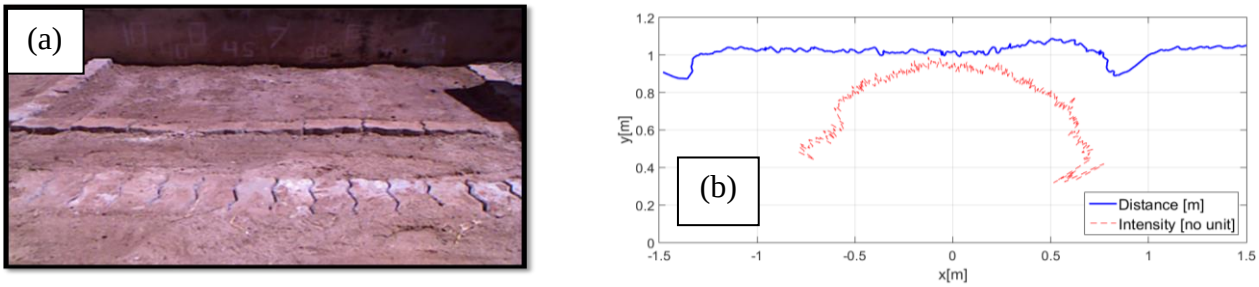

Figure 5. Day 2: readings at spot 1. (a) Kinect photo; (b) LiDAR readings

The photo shown in Fig. 6a was taken with Kinect when the wood stand was located at the spot 5 in the 8th day at 8 a.m. The LiDAR readings taken at the same spot and at the same time are shown in Fig. 6b. In this case, there are plants emerging from the ground which could be detected by the LiDAR (red circles in Fig. 6b. The two peaks represent a plant of the rows closed by red squares in Fig. 6a. Also, the detected plants generate two peaks in the LiDAR intensity readings (red graphic in Fig. 6b).

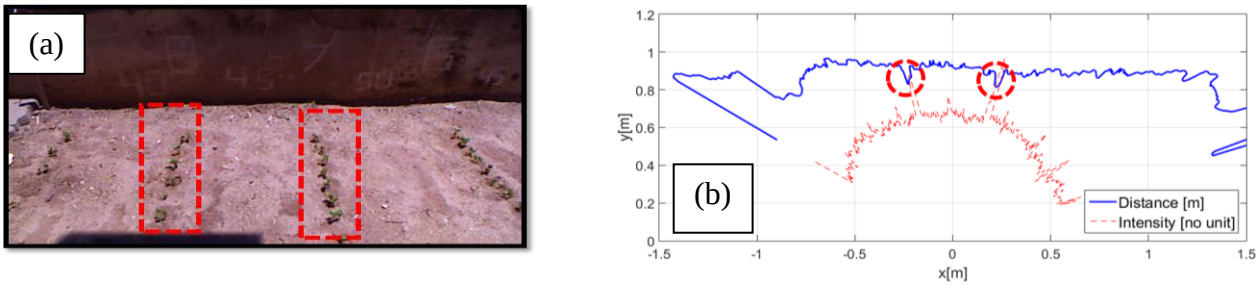

Figure 6. Day 8: readings at spot 5. (a) Kinect photo; (b) LiDAR readings

Figure 7a shows that the soybean plants in 20th day had a greater height than the last days. For this reason, the peaks presented in Fig. 7b are bigger. The photo and LiDAR readings presented in Fig. 7b were taken when the wood stand was located at the spot 5 in the 20th day at 8 a.m.

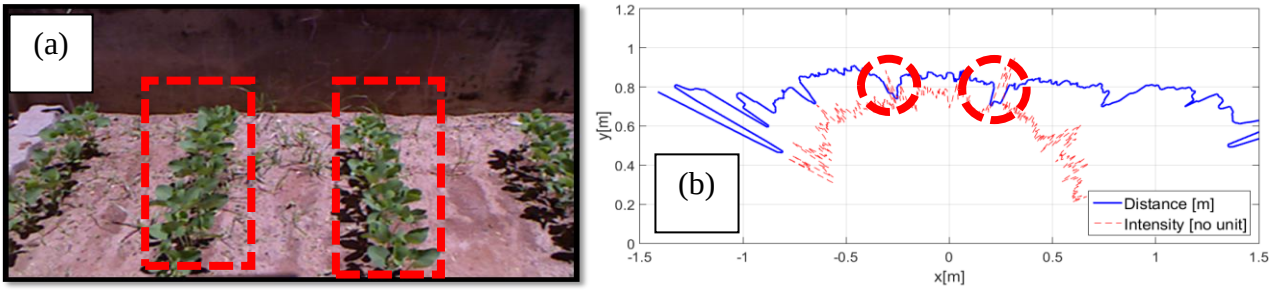

Figure 7. Day 20: readings at spot 5. (a) Kinect photo; (b) LiDAR readings

Finally, the behavior of the webcam was poor. In most of the tests, the webcam became saturated by the high intensity of light and it was impossible to obtain a clear image. This problem was most frequent in tests made between 12 am and 1pm. Although the Kinect always achieved to take a photo, the colors of this image varied depending of the day, hour and the climate. For rainy days, the colors were darker than on sunny days. LiDAR behavior was not affected by climate changes neither by the time. Beginning on the fifth day, the LiDAR sensor could detect the soybean plant. After 30 days, LiDAR intensity could not detect the plants anymore. It happened because the row spacing was reduced and the ground intensity was very similar to the plant intensity. After 40 days, the row spacing was totally reduced in the crop rows with row spacing equal to 0.4m and 0.45m. The plants of the crop rows with 10 plants per linear meter presented faster growth than the plants of the crop crow with 6 plants per linear meter.

4. CONCLUSIONS

Given a nominal usage of the robot components, the electrical autonomy of the robot is expected to be 63 minutes. Allied to 50kg payload, the robot stands as a moving platform for an ample range of sensors that can be used to provide information about agricultural field. Despite it will not be able to navigate in crops in R2 and R8 growth stages, the robot enables a fine acquisition of under canopy data while UAVs provides a whole season of over canopy information.

Moreover, the use of a passive suspension will allow the robot to adapt easier to the unevenness of the ground without using extra energy. Also, it compensates the inclination of the robot body generated by the unevenness of the ground, important to the use of the LIBS sensor.

Although in the initial days of the experimental soybean crop test, LiDAR intensity enabled the plants detection, it cannot be used after 30 days because the row spacing is reduced and the LiDAR intensity cannot differentiate between the plant and the ground. For this reason, the use of the LiDAR intensity is only recommended as a redundant indicator of plant present and also limited to initial days of plant growth.

As result of the test made in the experimental soybean crop, the use of Kinect and LiDAR sensors are recommended. The LiDAR presented the same behavior in all test and the Kinect did not suffer considerable anomalies in its behavior as it could be compared between images taken in hours with different luminosity intensities.

5. ACKNOWLEDGEMENTS

This paper was supported by grants no. 2016/09970-0 and no. 2017/10401-3, São Paulo Research Foundation (FAPESP). The authors also would like to thank FINEP, CNPq, CAPES, EMBRAPA and EESC-USP, for their support in this work.

6. REFERENCES

Advantech, 2016. “ARK-3510”. 28 Set. 2017 <http://advdownload.advantech.com/productfile/PIS/ARK-3510/Product%20-%20Datasheet/ARK-3510_DS(11.16.16)20161116101820.pdf >.

CONAB, 2016. “Acompanhamento da safra brasileira: Grãos”. 28 Set. 2017 <http://www.conab.gov.br/OlalaCMS/uploads/arquivos/16_06_09_09_00_00_boletim_graos_junho__2016_-_final.pdf >.

de Freitas, M.C.M., 2011. “A cultura de soja no Brasil: O crescimento da produção brasileira e o surgimento de uma nova fronteira agrícola”. *Enciclopédia Biosfera*, Vol. 7, p. 1-12.

Demski, P., Mikulski, M., Koteras, R., 2013. “Characterization of Hokuyo UTM-30LX Laser Range Finder for an Autonomous Mobile Robot”. *Advanced Technologies for Intelligent Systems of National Border Security*, Vol. 44, p. 143-153.

Dronelli, V., 2017. “8 drones that can lift heavy weigths [2017 edition]” 04 Out. 2017 < http://www.dronesglobe.com/guide/heavy-lift-drones/>.

EMBRAPA SOJA, 2010. "Cultivares de soja: regiões sul e central do Brasil". 28 Set. 2017 <http://www.cnpso.embrapa.br/download/FolhetoSoja.pdf >.

FAO, 2011. *The state of the World's land and water resources for food and agriculture-Managing systems at risk*. Organization of the United Nations and Earthscan, London and Rome, 1st edition.

FAO, 2015. *The State of Food Insecurity in the World*. Organization of the United Nations, Rome, 1st edition.

Farias, J. R. B., Nepomuceno, A. L. and Neumaier, N., 2007. "Ecofisiologia da soja". 28 Set. 2017 <https://www.agencia.cnptia.embrapa.br/Repositorio/circtec48_000g3bkhmrq02wx5ok0r2ma0nxz1b1po.pdf >.

Han, J., Shao, L., Xu, D. and Shotton, J., 2013. "Enhanced Computer Vision With Microsoft Kinect Sensor: A Review". *IEEE Transactions on Cybernetics*, Vol. 43, n. 5, p. 1318-1334.

Heiffig, L.S., Câmara, G.M.S., Marques, L.A., Pedroso, D.B. and Piedade, S.M.S., 2013. "Fechamento e índice de área foliar da cultura da soja em diferentes arranjos especias". *Bragantia*, Vol. 65, n. 2, p. 285-295.

Higuti, V.A.H., Guerrero, H.B., Velasquez, A.E.B., Pinto, R.M., Tinelli, L.M., Magalhães, D.V., Becker, M., Barrero, J.F. and Milori, D. M. B. P., 2015. "Low-cost embedded computer for mobile robot platform based on raspberry board". In *Proceedings of 23rd ABCM International Congress of Mechanical Engineering - Cobem2015*. Rio de Janeiro, Brazil.

Höfig, P., Araujo-Junior, C.F., 2015. "Classes de declividade do terreno e potencial para mecanização no estado de Paraná". *Coffee Science*, Vol. 10, n. 2, p. 195-203.

Hokuyo Automatic Co, 2012. "UTM-20LX_Specification". 28 Set. 2017 <https://www.hokuyo-aut.jp/dl/UTM-30LX_Specification.pdf>.

Larenas, M.C, Magalhães, D.V. and Milori, D.M.B.P., 2016a. "Sistema de enfoque automático para espectroscopia de plasma induzido por laserT". In *Proceedings of IX Reunion Ibero-americana de óptica y XII reunión Ibero-americana de óptica, lasers y aplicaciones – RIAO/OPTILLA2016*. Pucón, Chile.

Larenas, M.C, Magalhães, D.V. and Becker, M., 2016b. "Design of robotics arm for LIBS in field". In *Proceedings of 1° Simpósio do programa de pós-graduação em engenharia mecânica da EESC-USP – SiPGEM2016*. São Carlos-SP, Brazil.

Larenas, M.C, Milori, D.M.B.P. and Magalhães, D.V., 2016c. "Efeito da compactação do solo sobre o nível da sinal obtida por espectrometria de emissão óptica com plasma inducido por laser (LIBS)". In *Proceedings of 2° Simpósio do programa de pós-graduação em engenharia mecânica da EESC-USP – SiPGEM2017*. São Carlos-SP, Brazil.

Maxon motor, 2016. "EPOS2 24/5 Hardware reference". 28 Set. 2017 <https://www.maxonmotor.com/medias/sys_master/root/8821326184478/367676-Hardware-Reference-En.pdf>.

Maxon motor, 2016. "ESCON 50/5 Hardware reference". 28 Set. 2017 <https://www.maxonmotor.com/medias/sys_master/root/8818447482910/409510-ESCON-50-5-Hardware-Reference-En.pdf>.

Mazur, M., 2016. "Six ways Drones are Revolutionizing Agriculture". 04 Out. 2017 < https://www.technologyreview.com/s/601935/six-ways-drones-are-revolutionizing-agriculture/>.

Melorose, J., Perroy, R. and Careas, S., 2015. "World population prospects". United Nations, v. 1, n. 6042, p. 587–92, 2015. ISSN 1098-6596. Disponível em: <http://www.ncbi.nlm.nih.gov/pubmed/21798940>.

Ministério da Agricultura, Pecuária e Abatecimento, 2016. "Projeções do Agronegócio: Brasil 2015/16 a 2025/26". 28 Set. 2017 <http://www.agricultura.gov.br/assuntos/politica-agricola/todas-publicacoes-de-politica-agricola/projecoes-do-agronegocio/proj_agronegocio2016.pdf/view >.

Mundstock, C.M. and Thomas, A. L., 2016. "SOJA Fatores que afetam o crescimento e o rendimento de graõs. Porto Alegre". 28 Set. 2017 <www.ufrgs.br/agronomia/plantas/destaques/livro_soja.php>.

Pallejá, T., Teixidó, M., Tresanchez, M. and Palacín, J., 2009. "Measuring Gait Using a Ground Laser Range Sensor". *Sensors*, Vol. 9, n. 11, p. 9133-9146.

Ritchie, S.W., 1998. "Como a planta se desenvolve". 28 Set. 2017 <http://brasil.ipni.net/ipniweb/region/brasil.nsf/0/9EB3E1289BF2532B83257AA0003BF72A/$FILE/Como%20a%20Planta%20da%20Soja%20Desenvolve.pdf >.

Sparkfun, 2015. "SparkFun 9 Degrees of Freedom Breakout - MPU-9150". 28 Set. 2017 <https://www.sparkfun.com/products/retired/11486>.

Swift Navigation, 2017. "Piksi_multi_product_summary". 28 Set. 2017 <https://www.swiftnav.com/sites/default/files/piksi_multi_product_summary.pdf>.

Teixidó, M., Pallejá, T., Font, D., Tresanchez, M., Moreno, J. and Palacín, J., 2012. "Two-Dimensional Radial Laser Scanning for Circular Marker Detection and External Mobile Robot Tracking". *Sensors*, Vol. 19, n. 2, p. 4-10.

United Nations, 2015. "World population prospects. United Nations" v. 1, n. 6042, p. 587–92, 2015. ISSN 1098-6596. Disponível em: <http://www.ncbi.nlm.nih.gov/pubmed/21798940>.

Zhang, Z., 2012. "Microsof Kinect Sensor and its effect". *IEEE MultiMedia*, Vol. 19, n. 2, p. 4-10.

7. RESPONSIBILITY NOTICE

The authors are the only responsible for the printed material included in this paper.